Transcriptomic Evaluation of Stress Vulnerability Network using Single Cell RNA-Seq in mouse Prefrontal Cortex

Benjamin Hing[1]*, Sara Mitchell[1]*, Maureen Eberle[1], Yassine Filali[1,2], Molly Matkovich[1], Mukundan Kasturirangan[1], Ian Hultman[3], Whitney Wyche[1], Alli Jimenez[1], Radha Velamuri[1], Micah Johnson[1,2], Sanvesh Srivastava[3], Rainbo Hultman[1,4‡]

1 Department of Molecular Physiology and Biophysics, University of Iowa, Iowa City, IA, USA

2 Interdisciplinary Graduate Program in Neuroscience, University of Iowa, Iowa City, IA, USA

3 Department of Statistics and Actuarial Science, University of Iowa, Iowa City, IA, USA

4 Department of Psychiatry, University of Iowa, Iowa City, IA, USA

* Co-equal authors listed alphabetically. ‡ Correspond with Dr Hultman (Dept. of Molecular Physiology & Biophysics, Iowa Neuroscience Institute, 51 Newton Rd., 6-510 Bowen Science Building, Iowa City, IA, 52242, USA; 319-335-2855 (o), 919-451-6906 (c); rainbo-hultman@uiowa.edu.

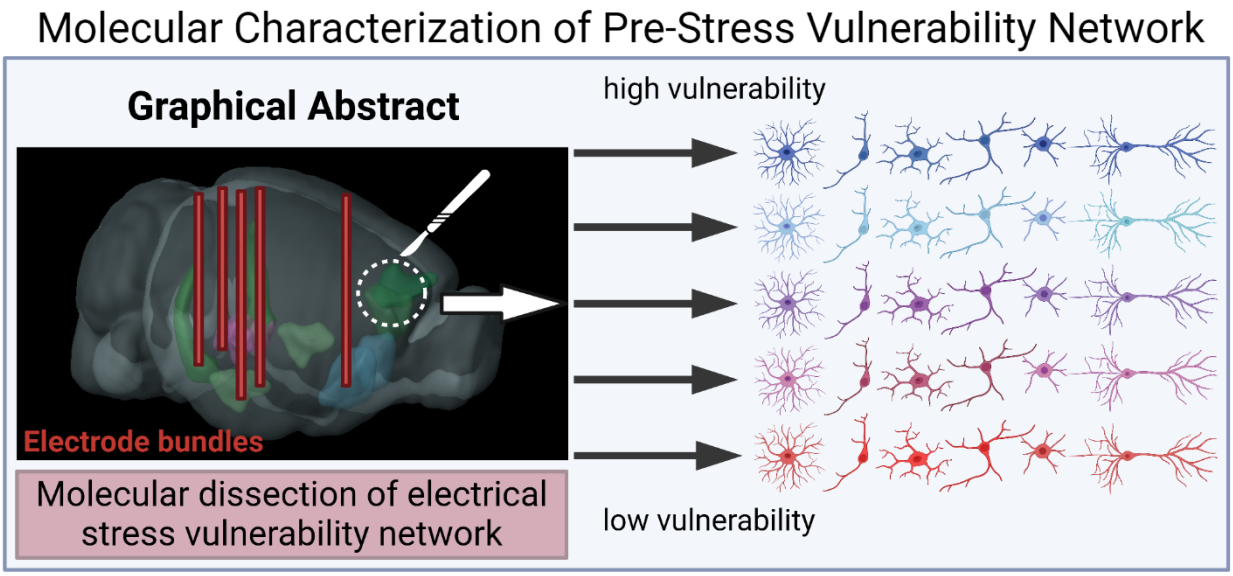

Abstract

Increased vulnerability to stress is a major risk factor for the manifestation of several mood disorders, including major depressive disorder (MDD). Despite MDD's status as a significant donor to global disability, the complex integration of genetic and environmental factors that contribute to the behavioral display of such disorders has made a thorough understanding of related etiology elusive. Recent developments suggest that a brain-wide network approach is needed, taking into account the complex interplay of cell types spanning multiple brain regions. Single cell RNA-sequencing technologies can provide transcriptomic profiling at the single-cell level across heterogenous samples. Furthermore, we have previously used local field potential oscillations and machine learning to identify an electrical brain network that is indicative of a predisposed vulnerability state. Thus, this study combined single cell RNA-sequencing (scRNA-Seq) with electrical brain network measures of the stress-vulnerable state, providing a unique opportunity to access the relationship between stress network activity and transcriptomic changes within individual cell types. We found especially high numbers of differentially expressed genes between animals with high and low stress vulnerability brain network activity in astrocytes and glutamatergic neurons but we estimated that vulnerability network activity depends most on GABAergic neurons. Furthermore, we found that genes significantly upregulated in animals with higher vulnerability brain network activity across multiple cell types included upregulation of microglia activity, mitochondrial and metabolic pathways, and those with lower vulnerability network activity included pathways involved in synapse regulation.

Intro

Stress has been demonstrated to be a major environmental contributor to myriad disorders, particularly mood disorders such as major depressive disorder (MDD) [1]. Most such disorders are polygenic, with greater numbers of SNPs increasing an individual's risk to psychiatric disease. Genes conferring risk work together in complex ways across different cell types, sometimes in near dose-dependent ways, suggesting that a more complete understanding of gene expression events will be necessary for understanding the etiology of such disorders [2-5]. This appears especially true for MDD, a psychiatric disorder for which heritability is most diverse and susceptible to environmental contributors such as stress [6, 7].

Toward this end, substantial progress has been made in understanding the gene regulatory events distinguishing stress-susceptible and resilient brain states in rodent models of depressive brain states [8, 9]. In particular, transcriptional regulation of the prefrontal cortex (PFC), has been shown to play an important role in mediating stress susceptibility and in disorders that can often be exacerbated by stress such as MDD [9-12]. At least five different cell types have been implicated in the etiology of stress susceptibility and related disorders such as MDD in the PFC including excitatory [13-16] and inhibitory [2, 17] neurons, astrocytes [18], oligodendrocytes [19], and microglia [20].

While it has long been recognized that stress has the potential to trigger or exacerbate negative affect states, the gene expression events defining the predisposing vulnerability state has not been rigorously characterized in the same way that post-stress susceptibility and resilience have. Previously, we used multi-site *in vivo* neurophysiology and machine learning methods to identify and validate a local field potential (LFP)-based brain network, *Electome Factor* 1, that could reliably identify a stress vulnerability state without the full manifestation of a stress-induced depressive state [21]. Here, we record *Electome Factor* 1 brain network activity and assess gene expression in specific cell types within the PFC of the

same animals, a key driving region of this vulnerability network, to provide a better understanding of the stress-vulnerable state as well as the gene expression architecture of this electrical brain network.

Material and Methods

Animals and Experimental Design:

All animals were housed in accordance with the University of Iowa Institutional Animal Care and Use Committee (IACUC) standards. All mice were housed in bedded cages and exposed to a 12-hour light/dark cycle with ad libitum access to food and water. This study utilized C57BL/6J mice delivered from the Jackson Laboratory in Bar Harbor, Maine at 5-7 weeks of age. Prior to surgery, experimental mice were group-housed by sex. Following surgical implantation of recording electrodes, experimental mice were singly-housed and placed on corncob bedding. Each implanted animal was exposed to a forced interaction test (FIT), a test designed to elicit a negative affect response, one time only: two days prior to sample collection for single-cell RNA sequencing (scRNA-seq) (Fig 1). Forty-eight hours after recording each FIT, the prefrontal cortex (PFC) was micro-dissected and processed for scRNA-seq.

Surgical Implantation of Electrodes:

For surgical implantation of recording electrodes, mice were anesthetized with 1-5% isoflurane, and their skulls were secured in a stereotaxic device. Metal ground screws were placed above the anterior cranium and the cerebellum before implanting target bundles. Electrode bundles designed to target the following regions: nucleus accumbens (NAc), amygdala (AMY, basolateral, BLA and central, CeA), ventral hippocampus (VHipp), and ventral tegmental area (VTA), were positioned according to stereotaxic coordinates measured from Bregma as previously described [22, 23]. These coordinates were chosen to maintain consistency with prior molecular and neurophysiology studies of vulnerability following chronic stress [9, 21]. The PFC (including prelimbic, Prl and infralimbic, IL components) was intentionally left out of the electrode design so as not to disturb the tissue that would later be collected for scRNA-sequencing. This was possible because *EF1* scores can still be calculated with minimal regions missing from the recording data [21]. Experimental animals were implanted between 6-10 weeks of age and were allowed to recover for a minimum period of 2-weeks prior to testing (Supplementary Figure 1). Accuracy of electrode placement during implantation was evaluated at the conclusion of the experiments through individual subject histological assessment. This was done to confirm the exact recording sites used to capture neurophysiological data.

Acquisition of Neurophysiological data:

Neurophysiological data was captured as previously described [21] for each subject during the completion of a forced interaction test (detailed below). The CerePlex Direct acquisition system was used to capture neuronal activity data sampled at 30kHz (Blackrock Microsystems, UT, USA). Acquired local field potentials (LFPs) were stored at 1000 Hz following a bandpass filter set at 0.5-250Hz. A ground wire connecting both ground screws served as an overall reference for neurophysiological recordings within each experimental animal.

Forced Interaction Test:

The forced interaction test (FIT) was performed as previously described [24] with recordings obtained from 5 brain regions over the duration of the FIT in addition to the capture of corresponding video for animal behavior (Fig 1A) [21]. Mice were first connected to a mu headstage and kevlar-coated cable (Blackrock Microsystems, UT, USA) before being placed in a fresh homecage with corncob bedding. Following a 30-minute habituation period, a 10-minute baseline homecage recording portion of the FIT was performed. An 18” high, clear, acrylic cage extender was placed just inside the walls of the home cage to prevent the implanted animal from climbing out. Succeeding the homecage recording, the

experimental animals were placed in a 3.25" diameter x 7" high covered Plexiglass carousel (Noldus) while neurophysiological data was collected for a period of 5 minutes. A CD1 mouse previously screened for aggressive tendencies was then placed inside the cage extender, but outside the carousel within the homecage, and the recording continued for an additional 5 minutes. The carousel was designed to protect experimental animals from outside harm, while maintaining sensory interactions with the outside environment through the presence of open-air slots. Experimental mice were only subjected to the FIT once, a minimum of 2 weeks following surgical implantation of electrodes to allow for sufficient recovery, and always 2 days prior to tissue collection for scRNA-seq sample prep. FIT recordings and subsequent sample collections were performed when animals were between 9 and 14 weeks of age (Supplemental Figure 1). The local field potentials (LFPs) obtained from the FIT recordings were evaluated for each mouse to determine their *Electome Factor 1* (*EF1*) scores, a previously identified marker of the stress vulnerable state (see below).

Buffer Preparation, Tissue Collection, and Generation of Single-Cell Suspensions:
Artificial cerebrospinal fluid (NMDG-aCSF) buffer was freshly prepared on the day of harvesting cells and contained the following powdered reagents, in order: 96 mM NMDG (Sigma-Aldrich; St. Louis, MO; CAS No. 6284-40-8,), 2.5 mM KCl (Research Products International; Mt. Prospect, IL; CAS No. 7447-40-7), 1.35 mM NaH_2PO_4 (Sigma-Aldrich; St. Louis, MO; CAS No. 7558-80-7), 30 mM $NaHCO_3$ (Research Products International; Mt. Prospect, IL; CAS No. 144-55-8), 20 mM HEPES (Research Products International; Mt. Prospect, IL; CAS No. 7365-45-9), 25 mM glucose (Research Products International; Mt. Prospect, IL; CAS No. 50-99-7), 5 mM Na+ascorbate (Sigma-Aldrich; St. Louis, MO; CAS No. 134-03-2), 2mM thiourea (Sigma-Aldrich; St. Louis, MO; CAS No. 62-56-6), 3 mM Na+pyruvate (Sigma-Aldrich; St. Louis, MO; CAS No. 113-24-6), 2 mM N-acetyl-L-cysteine (Sigma-Aldrich; St. Louis, MO; CAS No. 616-91-1). Powdered reagents were measured using weigh boats and poured into a 500mL graduated cylinder one at a time; excess material was washed into the graduated cylinder using ddH20. Following the addition of all powdered reagents, the solution was then adjusted to 80% final volume with ddH20. Under the fume hood, the liquid reagents were then added directly to the solution using a P1000 pipette, in the following order: 37% HCl (Sigma-Aldrich; St. Louis, MO; CAS No. 7647-01-0), 0.5 mM CaCl2 (Alfa Aesar; Ward Hill, MA; CAS No. 10043-52-4), 10 mM MgSO4 (GBiosciences; St. Louis, MO; Cat. # 786-530). The final volume of the solution was then adjusted to 500mL using the ddH20 spray bottle. After adding a stir bar into the solution and covering it with parafilm, the graduated cylinder was placed atop a stir plate, and all reagents were allowed to dissolve into the solution at 300-350 rpm for 10 minutes. The incorporated NMDG-aCSF solution was then filtered through a 100µm Nylon cell strainer (Falcon; Corning, NY; Ref: 352360) into an Erlenmeyer flask, covered with parafilm, labeled, and either stored at 4°C overnight or prepared for use as follows.

NMDG-aCSF, prepared within 24-hours of planned collections, was bubbled in carbogen (95% O2/5% CO2) for at least 75 minutes on ice prior to contacting any tissue samples. During this time, Earle's Balanced Salt Solution (EBSS) solution and albumin inhibitor solution were also bubbled on ice, which was maintained throughout the duration of the experiment, taking care to prevent the formation of bubbles in the albumin inhibitor. After the NMDG-aCSF had been bubbling for 75-100 minutes, the pH was measured to be 7.35-7.45 and the osmolarity was measured to be 300-310 mOsm. If pH or osmolarity measurements fell outside of their respective range, then the buffer was not used for sample processing.

Animals were anesthetized using Euthasol (Virbac AH, Inc.; Fort Worth, TX) and perfused with ice cold NMDG-aCSF. Their brains were rapidly removed, adhered to a rotating specimen disk using Loctite® 404™ Quick Set™ Instant Adhesive (Henkel; Rocky Hill, CT; P/N 135465), placed in a cold bath of

bubbling NMDG-aCSF buffer on a Leica VT1200 vibratome (Leica Biosystems; Ref: 14048142065) and sliced coronally in200µm slices. Exactly six slices were used for each brain's PFC dissection. Ice was used to keep the samples cold whenever possible in all proceeding steps.

The slices were transferred to recovery holding strainers secured in 6-well plates and bubbled in NMDG-aCSF. Slices were allowed to recover for 10-15 minutes. Papain solution was prepared by adding oxygenated cutting solution to the papain and incubating this without agitation at 37°C for 10 minutes. Five minutes into the papain incubation, oxygenated EBSS was added to the DNASE, mixed by inversion, and placed on ice. After 10 min of papain incubation, the papain was combined with the prepared DNASE, mixed by inversion, and left at room temperature. While the papain was being prepared, the slices were micro-dissected (see Supplementary Figure 3) using a scalpel and dissection scope (Jewelmont) with a halogen cool light source (AmScope; SKU: HL250-AY; Irvine, CA) and transferred to a microcentrifuge tube. The NMDG-aCSF was then carefully removed from the tube containing the micro-dissected tissue, being replaced by the addition of the papain solution.The tissue was incubated in the papain solution for 30-40 minutes at 37°C at 60 RPM using an Innova 4000 Incubator Shaker (New Brunswick Scientific; Enfield, CT; P/N: NB-4000). The papain solution was removed from the tissue and diluted albumin inhibitor (stop solution) was added. Triturations were carried out using two sequential bore diameters (~300µm and ~150µm) of fire-polished glass capillaries (World Precision Instruments; Sarasota, FL, Item No. TW100-3). A total of six triturations were used for female mice and twelve triturations for male mice, with the first half completed using the 300µm bore capillary and the latter half with the 150µm bore capillary. After the mechanical dissociation was complete, the resulting suspension was cloudy and homogenous. The suspension was filtered through a 40um mesh filter (Falcon, Corning NY; Ref: 352340), and then transferred to a 15mL conical tube and centrifuged at room temp., 0.1 RCF for six minutes. Following centrifugation, the supernatant was quickly but carefully removed. Using a P1000 wide-bore tip, the pellet was resuspended in 1mL of stop solution (aspirated and suspended about five times) and then filtered through another 40µm mesh Falcon cell strainer. In another conical tube, 5mL of stop solution was added, and the cell suspension was carefully layered on top using a P1000 wide-bore tip. This suspension was again centrifuged at room temp, 0.1 RCF for six minutes. Following the second centrifugation, a P1000 wide-bore tip was used to remove the supernatant until about 50µL of the solution was left. Then, using a P200 tip, 20-30µL of the solution was removed until about 20µL of cell suspension remained. The pellet was then resuspended in 30µL HBSS to generate the final single-cell suspension.

Cell Counting

Equal volumes of single-cell suspension and 0.4% trypan blue stain (Life Technologies corporation; Grand Island, NY; Ref: 15250-061) were mixed and 10µm of the resulting solution was loaded onto a hemacytometer (Hausser Scientific; Horsham, PA; Cat No. 02-671-10). A Leica DMi1 inverted microscope (Leica Biosystems; Ref: 11526227) was used to view the counting chamber using an S40-slider (Leica Biosystems; Ref: 1152613). Both live and dead cell counts were obtained from each of the four corners of the chamber's etched grid to determine total cell density as well as the percentage and total of live cells present in the single-cell suspension.

Projecting Neurophysiological Data into 'Electome Factor Space'

LFP data acquired from the FIT recordings were used in conjunction with the learned feature representation from a previously developed machine learning model using "discriminative cross-spectral factor analysis" (dCSFA) to calculate vulnerability scores (*Electome Factor* 1) [21]. The LFP oscillations obtained from our experimental mice were projected into the space of the *Electome Factors* that were previously learned as previously described [21].

Single cell library preparation and sequencing

Single cell libraries were generated using the Chromium Next GEM Single Cell 3' Kit v3.1 as per manufacturer's instructions and sequenced using the Illumina NovaSeq6000 using 100 bp paired-end reads at the University of Iowa Institute of Human Genetics Genomics Division. Raw base call files were demultiplexed and FASTQ files were generated using the Cell Ranger program (10X Genomics).

Quality control, clustering and celltype identification

FASTQ files (N=168) were evaluated using FastQC (v0.11.7) and MultiQC (v1.5) to determine excellent sequencing quality (Phred score > Q30). The cellranger count function from Cellranger-6.0.0 was used to align the FASTQ files to the mouse reference genome (mm10; pre-built reference mm10-2020-A obtained from the 10X genomics website) and for feature quantification. The average number of reads per cell was ~ 97,000 reads (Supplementary Table 2). Cellranger aggr was performed with the argument '--normalize mapped ' to aggregate the data. Data was subsequently loaded into RStudio (4.1.1) and processed using Seurat (4.1.1) for normalization, data reduction, clustering, and visualization. Briefly, high quality cells defined by percentage mitochondria < 10% [25] and total feature counts > 1000 were retained for downstream analysis. The SCTransform function was used to normalize the data and control for confounding sources of variation such as read depth and mitochondria percentage. Based on knee plots, 15 principal components were used to create a shared nearest neighbor graph. Cells were clustered into groups by optimizing a modularity function (Louvain algorithm, resolution 0.8, 10 random starts and 10 iterations). Data was visualized using t-distributed stochastic neighbor embedding (tSNE) plots. Doublets were identified using scDblFinder (1.8.0) [26] and removed from the analysis. The number of doublets was ~ 2% which is consistent with the expected number of doublets for 10X single cell RNA-Seq as per manufacturer's guidelines. Cluster identity was determined by cell type specific marker gene expression including glutamatergic neurons (*Slc17a7* and *Slc17a6*), GABAergic neurons (*Gad1* and *Gad2)*, astrocytes (*Aldoc* and *Apq4)*, mature oligodendrocytes (*Mbp* and *Cldn11*), oligodendrocyte precursors (*Pdgfra),* endothelia (*Pecam1* and *Slc2a1)*, microglia (*Tmem119)*, pericytes (*Vtn)*, endothelia (*Pecam1* and *Slc2a1*) and vascular smooth muscle (*Tagln)*. To further validate the identity of the cells in each cluster, the cell2cluster function from the scmap package (version 1.16.0) was used together with a prefrontal cortex (PL-ILA-ORB) reference dataset extracted from the 10X single cell RNAseq dataset from the Allen Brain Atlas [27]. Cells that were not consistent with the identity of their cluster were removed from the analysis. Similarly, a cluster that ambiguously co-expressed markers for endothelial and pericytes was also removed from the analysis.

Hierarchical clustering

Electome Factor 1 (*EF*1) score was used to calculate the Euclidean distance followed by hierarchical clustering using the complete-linkage method.

Differential gene expression

The differential gene expression analysis of the scRNA-seq results were limited to those animals having either high or low EF1 scores, excluding those with intermediate scores (Figure 1D). Only cell types with at least 10 cells per individual mouse was used for differential gene expression (DEG) analysis using corrected counts obtained from SCTransform as a recent study showed that this reduces false positive rates [28]. All mitochondria transcribed genes were removed prior to DEG analysis. Analysis was performed using ZINB-WaVE-DEseq2 workflow [29]. Size factors were computed using computeSumFactors [30]. Significance testing was performed using the likelihood ratio test to evaluate the effects of EF1 while controlling for sex as a covariate in the full model (~ EF1_level + Sex) and compared against the reduced model (~ Sex). Additional arguments included in the Deseq function were

useT=TRUE, minmu=1e-6, minRep=Inf and sfType="poscounts" as per recommendation in the DESeq2 and ZINB-WaVE vignettes and other studies [29, 31-33]. In order to assess the validity of the SINB-WaVE differential gene expression, the package DESingle [34] was also used for DEG analysis as it is comparatively as good or better in performance compared to other algorithms [35] and we have successfully used this method for DEG analysis in a previous study [36]. Genes with FDR < 0.05 were differentially expressed.

Gene Ontology analysis

Gene ontology analysis was performed using clusterProfiler (version 4.2.2) [37] to identify biological processes that were over-represented for genes that were differentially expressed. We also used SynGO [38] to identify over-representation of genes for biological processes and cellular components related to the synapse.

Gene Set Enrichment Analysis

Normalized gene expression counts from DESeq2 was used for gene set enrichment analysis (GSEA). Analysis was performed using GSEA (version 4.2.1) with the gene ontology biological processes dataset (C5) containing 7751 gene sets from the Molecular Signatures Database or using mitochondria reference dataset from the MitoCarta 3.0 [39]. Mouse gene symbols were remapped to their human orthologs using GSEA program and we also used the following settings: phenotype for permutation type, enrichment statistic was classic and metric for ranking genes was Singal2Noise.

Results

The overall goal of these experiments was to identify gene expression underlying a previously defined stress-vulnerability brain state, a brain state recognized to predispose animals to manifesting a depressive phenotype following stress [21]. A neurophysiological metric of the stress vulnerability state was used, *Electome Factor 1*, characterized by local field potential (LFP) features spanning seven brain regions: prelimbic (PrL) and infralimbic (IL) cortices, nucleus accumbens (NAc), basolateral (BLA) and central (CeA) amygdala, ventral hippocampus (Vhipp), and ventral tegmental area (VTA). A complete set of these features is outlined in Figure 1B and Supplementary Figure 2. Having previously established that the strength of this network signature can be measured over time using a subset of just five brain regions, in the current study we implanted 6 male and 6 female C57BL/6 animals in NAc, BLA, CeA, VTA, and vhipp [21]. We carried out a forced interaction test (FIT) and calculated *Electome Factor 1* using a previously developed method of projecting new data onto our previously developed stress *Electome Factor* features (Figure 1A, B) [21]. We then dissected prefrontal cortex (PFC), which included PrL and IL for single cell RNA-Seq.

In order to identify differential gene expression differentially regulated between animals with high and low stress-vulnerability electrical brain network activity (*Electome Factor* 1), we clustered *Electome Factor* 1 scores using a hierarchical clustering method (Figure 1D). We identified three animals with the lowest *Electome Factor* 1 scores (i.e. corresponding with more stress-resistance) and four animals with the highest *Electome Factor* 1 scores (i.e. corresponding to the more stress-vulnerable, Figure 1E). *Electome Factor* 1 scores over time on the forced interaction test (FIT) are shown in Figure 1C.

Identification of cell types in the PFC

Single cell analysis identified clusters corresponding to nine major cell types in the PFC (Figure 2A-B, Supplementary Figure 5). Their distribution was not influenced by factors such as sex, *EF*1 score and

experimental dates (Figure S6). The proportion of these cell types were similar between males and females (Figure 2C) and is in line with other studies [40, 41]. While the proportion of these cell types did not differ between high and low *EF*1 groups, GABAergic neurons had a significantly higher proportion (FDR < 0.05) in *EF*1 high group compared to *EF*1 low group (Figure 2D).

Single Cell Gene Expression Analysis

To evaluate how genes are differentially regulated in the PFC of high and low *EF*1 groups, differential gene expression was performed on cell types which have a minimum of 10 cells for all samples (Supplemental Table 3). Analysis was performed using the zero-inflated negative binomial model (ZINB)-WaVE-+ DEseq2 workflow. ZINB-WaVE is a flexible scRNA-Seq signal detection method that has been shown to provide accurate and stable representations of data at low dimensions, while eliminating the need for preliminary normalization [33]. To limit the influence of technical variation in the analysis, mitochondrial derived genes were removed from the data and we used counts corrected for mitochondria percentage obtained from SCTranform for the analysis.

Glutamatergic neurons had the greatest number of significant differentially expressed genes, with 838 genes significantly more highly expressed in the PFC of mice with high *EF1* scores, (Table 1, Figure 3A, Supplemental Table S7). Gene ontology (GO) analysis of these genes showed significant over-representation in biological processes including mRNA processing, respiratory processes and mitochondria related processes (Figure 3B and Supplemental Table 5). In contrast, 548 were significantly more highly expressed in mice with low *EF1* scores. Analyses by GO showed significant over-representation in biological processes involved with synapse organization and regulation (Figure 3C and Supplemental Table 5). To further support this result, we performed gene set enrichment analysis (GSEA), which is a threshold-free approach to identifying changes in biological processes between groups [42]. Consistent with the GO analysis, mice with high *EF*1 scores were significantly enriched for biological processes involved in respiratory and mitochondria related processes (Supplementary Figure S10). Mice with low *EF*1 score did not have significant enrichment for biological processes after correction for multiple testing. The top enrichment terms that trended towards significance included neuronal and synapse related function such as synaptic transmission of glutamatergic (FDR = 0.065), synapse assembly (FDR = 0.066) and glutamatergic receptor signaling pathway (FDR = 0.075).

The cell type with the second-highest number of DEGs was astrocytes. There were 341 genes significantly highly expressed in mice with high *EF*1 (Table 1, Figure 4A). GO analysis showed significant over-representation of these genes in biological processes including ribosomal and mitochondria related processes (Figure 4B and Supplemental Table 5). Conversely, there were 221 genes significantly highly expressed in mice with low *EF1* scores. Analysis by GO showed over-representation of these genes in neuronal related processes including various synaptic processes, regulation of synapse, neurotransmitter secretion and transport (Figure 4C, Supplemental Table 5). In line with the GO analysis, GSEA also showed significant enrichment of respiratory, and mitochondria related processes in the high *EF*1 group (Supplementary Table 5). GSEA also supported the findings of the GO analysis in the low *EF*1 group, as there was significant enrichment of neuronal related processes including synapse organization, assembly and synapse signaling (Supplemental Table 5).

Differential gene expression analysis of GABAergic neurons identified 242 genes that were significantly more highly expressed in the high *EF*1 mice (Table 1, Figure 3D). As with analyses of glutamatergic neurons and astrocytes, analysis of genes significantly more highly expressed with *EF*1 in GABAergic neurons by GO revealed significantly over-representation of these genes in biological processes involved in cellular respiration, oxidation, metabolism and mitochondria related processes (Figure 3E,

Supplemental Table 5). By comparison, there were 140 genes significantly highly expressed in the low *EF*1 group. Biological processes evaluated by GO analysis showed significant over-representation of these genes in neuronal related processes including axonogenesis, synapse organization and assembly, ion transport and cognition (Figure 3F, Supplemental Table 5). This result was also verified by GSEA which showed significant enrichment of terms for the high *EF*1 group which includes cellular respiration and mitochondria related processes (Supplemental Table 5). Similarly, the low *EF*1 group showed significant enrichment for neuronal related processes such as regulation of synapse function, synapse assembly and synapse organization (Supplemental Table 5).

Differential gene expression was performed on microglia, which showed 46 genes significantly more highly expressed in the high *EF*1 group (Table 1, Figure 4D). While GO showed over-representation of these genes in processes involved in the endoplasmic reticulum stress response and synapse pruning, it also highlighted processes involved in proinflammation such as cellular response to IL7, lymphocyte mediated immunity and regulation of actin filament organization (Figure 4E, Supplemental Table 5). In contrast, there were 77 genes with significantly higher expression in the low *EF*1 group. Analysis by GO showed a significant over-representation of these genes in processes involved in the regulation of synapse activity including synapse vesical cycle, synapse vesical cycle, synaptic vesical endocytosis and regulation of neurotransmitter levels (Figure 4F, Supplemental Table 5). In addition to GO analysis, GSEA also observed significant enrichment of cellular respiration and mitochondria related function in the high *EF*1 group (Supplemental Table S5 and Supplementary Figure S10). By comparison, the low *EF*1 group had significant enrichment of processes involved in neuronal processes such as the generation of neurons, developmental growth, and neurogenesis (Supplemental Table 5 and Supplementary Figure S10).

Finally, we also evaluated differential gene expression of mature oligodendrocytes. We observed 23 genes that were significantly highly expressed in the high *EF*1 group (Table 1, Figure 4G). Analysis by GO showed over-representation in processes involved in protein folding (Figure 4H). By comparison, there were 37 genes significantly highly expressed in the low *EF*1 group (Figure 4I) which were over-represented in processes involved in neuronal transmission processes including neurotransmitter secretion, signal release from synapse and regulation of neurotransmitter levels. GSEA analysis showed significant enrichment in processes involved in cellular respiration, metabolic processes and mitochondrial function for the high *EF*1 group (Figure and Supplemental Table 5). In contrast, there was an enrichment of neuronal processes including cell signaling, neuron generation and development (Figure and Supplemental Table 5).

Given that mitochondria related function was enriched in the high *EF*1 group across all cell types, we sought to further scrutinize this result by performing GSEA using a curated mitochondria dataset from MitoCarta which is a database that catalogs mitochondria related proteins and pathways [39]. We reasoned that if our findings of mitochondrial significance were truly specific to the high *EF*1 state, we would only see mitochondrial enrichment in pathways for the high *EF*1 group and not for the low *EF*1 group. GSEA showed enrichment of mitochondria related pathways in all five cell types mentioned above in the high *EF*1 group. There was however no enrichment in the low *EF*1 group. (Supplemental Table 6).

<u>Validation of differential gene expression analysis</u>

To verify that our approach of using ZINB-WaVE + DEseq2 analysis to identify differentially expressed genes is sound, we performed differential gene expression analysis using an independent program DESingle, an R package that utilizes a zero-inflated negative binomial model to distinguish between actual zero expression and technical dropout zeros for the detection of various DEGs in scRNA-Seq data

with improved accuracy [34]. Not only did the DEGS detected by DESingle align with ZINB-WaVE + DEseq2 in terms of the ranked quantity of DEGs detected by cell-type (Table S10, Figure S9), but the DEGs identified from the ZINB-WaVE + DEseq2 also largely overlapped with those detected by DESingle analysis (Figure 5). Using DEGs detected by DESingle, GO analysis of genes more highly expressed in the high *EF*1 group showed similar over-representation of biological processes as reflected in our initial analysis including metabolism and mitochondria related processes (Supplementary Figure S10, Supplemental Table 13) for glutamatergic neurons, GABAergic neurons, and astrocytes. By comparison, GO analysis of genes more highly expressed in the low *EF*1 group showed over-representation in processes involved in synaptic functions including synapse organization, assembly, axonogenesis, and synaptic vesicle cycle for all the cell types (Supplementary Figure S10, Supplemental Table 13).

When GO analysis was performed using genes that overlapped between both analysis methods, we observed a similar result whereby genes more highly expressed in the high *EF*1 group were over-represented in processes such as cellular respiration and mitochondria processes for glutamatergic neurons, GABAergic neurons and astrocytes (Supplementary table 14). There was also an over-representation of these genes in ribosomal processes in astrocytes. For microglia, there was over-representation of genes involved in proinflammation and immunoactivation processes including positive regulation of tumor necrosis factor, antigen processing and presentation of peptide antigen, positive regulation of interleukin 6 and positive regulation of phagocytosis (Supplementary table 14). In contrast, genes more highly expressed in the low *EF*1 group were over-represented for processes involved in regulation of neuronal or synaptic activity in all major cell types (Supplementary table 14).

Given our analysis had shown enrichment for processes involved in synapse regulation in the low EF1 group across all cell types, we sought to validate this further by performing an over-representation analysis using SynGO - a database containing expert curation of genes/proteins pertaining to the ontologies for the synapse [38]. Consistent with our GO and GSEA analysis, we observed significant over-representation of genes highly expressed in the low EF1 group for biological processes and cellular components related to synapse function for all cell types. In contrast, this over-representation was observed to a lesser degree of not observed for genes more highly expressed in the high EF1 group for the different cell types.

<u>Comparison of differentially expressed genes with those from chronic stress paradigm</u>
Since vulnerability increases the risk for susceptibility to chronic stress, we sought to compare our data to post-stress bulk RNA-Seq data from the PFC. Our rationale was that identifying genes that are more highly expressed in a pre-stress vulnerability brain state may help to identify which genes are already differentially regulated prior to stress and thus more likely to be causal than compensatory to the effects of stress. Specifically, we compared how genes more highly expressed in high *EF*1 mice would compare with DEGs obtained from the PFC of mice that are susceptible to chronic social defeat stress (CSDS) vs. those that are resilient [9]. To do this, we used previously published data from Bagot at al., which evaluated post-stress transcriptional differences in gene expression between susceptible and resilient animals at three time points: 48 hours after chronic stress, 28 days after chronic stress, and 28 days plus one hour after an additional bout of stress. We observed few DEGs that overlap with our dataset for susceptible mice that were assessed 48 hours after CSDS. However, at 28 days after CSDS, we observed 11 genes for glutamatergic neurons, 6 for GABAergic neurons, 31 for astrocytes and 2 genes for mature oligodendrocytes that overlapped with our dataset (Supplemental Table 7, column K). Analysis by GO for the overlapping genes in glutamatergic neurons and astrocytes showed over-representation of these genes in ribosomal processes (Supplemental Table 7). In contrast, there was

little to no overlapping genes with mice primed with previous CSDS exposure and that underwent an additional session of CSDS.

Discussion

Here we have implemented a novel approach combining multi-site in vivo neurophysiology with single cell transcriptomics to provide what to our knowledge is the first single cell resolution molecular characterization of a stress vulnerability brain state. We focused our study on the PFC both because of our previous findings of the importance of the PFC to the electrical network (EF1) defining the latent vulnerability state and because of the important role that the PFC plays in regulating stress responses, which suggested to us that understanding its gene regulation in an early stress-vulnerable state may be particularly illuminating [21, 43]. Notably, the differential gene expression identified here does not represent a response to a stressor or molecular manipulation but rather endogenously pre-existing differences between brains with more or less stress vulnerability electrical brain network activity. Nonetheless, we identified robust gene expression differences in these endogenous high and low *EF*1 activity states across all five of the major cell types we examined.

Beyond the effects observed across all cell types, several observations pointed toward a particular contribution of GABAergic cells to the stress vulnerability brain state defined by *EF*1. For one, GABAergic cells were the only population of cells with significantly different percentage representation between high and low EF1 groups (Figure 2D). When considering the overall contribution of different cell types to EF1 scores, we used a Gaussian Process model with principal component values for each cell type.. While we observed a similar strength of the correlation between *EF*1 activity and the first two principal components of gene expression of most cell types, GABAergic cells demonstrated a notably stronger relationship than the rest (Supplemental Methods and Results, Supplemental Table 16 and Supplementary Figure S16). This finding suggests that GABAergic neurons of the PFC may be the cell type with the most robust contribution to a given animal's *EF*1 score, and thus, predictive of their pre-stress vulnerability. Given the important role that inhibitory interneurons have been demonstrated to have both in regulation of LFPs, and in stress response and susceptibility, these results were not surprising.

Many rodent studies have shown that early life experiences and adverse exposures can impact GABAergic processes in the PFC, including maturation [44], inhibitory circuit development with the BLA and associated perineuronal net formation [45], and the programming of GABA transmission [46]. Along these lines, it has been found that chronic stress affects both the structure and function of prefrontal GABAergic networks [47, 48], with certain GABAergic sub-types showing enhanced vulnerability to stress [49]. Interestingly, and in further support of this point, we found trending differences in observed percentage of two GABAergic neuron sub-types: Pvalb and Vip, according to high and low *EF*1 score (Figure S8). Furthermore, there is myriad additional evidence supporting GABAergic neuronal features playing an important role in mediating stress resilience and susceptibility such as expression level of specific GABA receptors [50], signaling peptides [51], and subtypes [17], as well as interactions with the stress response pathway [52] [53] and the gut-vagus-brain pathway [54]. Although the aim of this study was to evaluate PFC cell-type specific gene expression in relation to a brain-wide network signature of pre-stress latent vulnerability, the broad association of GABAergic neurons in the PFC with stress and behavior provides considerable support for GABAergic neurons being a key contributor to *EF*1 activity.

Generally, however, the overall data suggests that it is the coordination of gene expression coming from multiple cell type network components and not one in particular that are responsible for generation of

the *EF*1 network. Given the important role of multi-brain region networks in both transcriptional and neural activity regulation of stress states [9, 21], future studies will be aimed at further mapping across multiple brain region states.

In line with this idea of coordinated multicellular network contributions to the vulnerability brain state, our analysis further showed distinct differences in function of different cell types between mice of opposing levels of stress-vulnerability. The PFC of mice which were more likely vulnerable to stress, as reflected by their high *EF*1 score, were enriched in processes such as cellular respiration, ribosomal function, mitochondria activity, and microglia activation. In contrast, mice which demonstrate less stress vulnerability brain activity (i.e. lower *EF*1 scores) have cell transcriptional states involved in synaptic processes for neuronal activity across all cell types.

While the number of studies that have broached studying this latent vulnerability state is small, there are several studies of note in the context of which we interpret our findings. These studies include identification of a stress vulnerability state via behavioral, neural circuit, and peripheral identifiers [55-58]. Encouragingly, our findings are largely consistent with the findings in these studies. For example, a previous study showed that IL-6 levels from peripheral blood or by ex vivo stimulation of leukocytes could predict susceptibility or resilience to a subsequent stressor. By replacing the peripheral immune system in stress-naïve mice with those from stressed animals, this could increase their susceptibility to repeated social defeat stress [55]. While this study addresses induction of vulnerability peripherally and our study measures gene expression in the PFC, our data are consistent with this picture of increased immune response in the latent stress vulnerable state. We observed gene expression consistent with increased activity of microglia, the cells of the brain resident immune system. We observed gene expression altered toward proinflammation and immune activation in mice with high *EF*1 activity. Many studies have shown that negative stressors can induce microglia activation (PMID: 31847911) which can rewire and impair neurocircuits [59, 60] and is linked with various psychiatric disorders [61, 62]. To our knowledge, this is the first study to report microglia activation in the brain (and specifically PFC) of stress-naive vulnerable mice. However, regulation of microglia in PFC following chronic social defeat stress has been linked to stress susceptibility [63]. Also, many studies of prenatal stress or early life adversity, which are often precursors to a vulnerable state, are consistent with our findings suggesting an important role for activated microglia in conferring vulnerability to stress [64-67].

In addition to microglia activation, our data also highlighted altered cellular respiration and mitochondria activity across all cell types in mice with high EF1 activity. While we had removed all mitochondrial derived genes from our analysis, there are genes involve in mitochondria function that are derived from the nucleus [68]. Mitochondria provide the energy that fuels enzymatic reactions for neuronal processes, which can affect stress response and behavior[69]. For example, a study where C57BL/6J mice were substituted with mitochondria containing a mutation that leads to the increased production of reactive oxygen species resulted in altered stress response, anxiety-like behavior and altered corticosterone regulation [70]. Other studies have also linked mitochondria dysfunction to depression and other mood and psychiatric disorders where stress frequently plays an important role [71-74]. Gene expression studies of major depressive disorder have link mitochondrial gene expression in the PFC with depression [75]. In fact, a mitochondrial metabolite has been identified that significantly alters neuroplasticity in the PFC and hippocampus, with promising data suggesting its as a therapeutic target for depressive disorders [76-78]. Follow up studies have found that factoring in mitochondrial and

metabolic measures alongside early life stress experience can enhance prediction of antidepressant response [79].

Importantly, recent studies have linked mitochondria function to stress susceptibility [80-82]. For example, mice exposed to chronic mild stress showed that susceptible and resilient mice had different expression of proteins involved in the mitochondria respiratory chain and mitophagy markers in the ventral hippocampus [82]**.** Similarly, a genome-wide study of gene expression in the PFC and NAc revealed that mice exposed to multimodal chronic stress had altered expression of mitochondria genes in the PFC of susceptible mice and the mitochondria gene expression profile correlated with behavior in these mice [83]. Given that these studies highlight the role of mitochondria in regulating behavior, our finding that respiratory and mitochondria processes are being upregulated in mice with high EF1 activity suggests that altered mitochondria could contribute to vulnerability to stress prior to stress exposure.

Given that our differential gene expression profile is connected to stress vulnerability, we wanted to evaluate how this would correspond with gene expression profiles of mice that were susceptible to stress after stress exposure. Although we saw a few overlapping genes between our data set and those of Bagot et al [9], one possible explanation for this could be due to comparison our single-cell resolution findings to data collected from bulk RNAseq dataset. In line with this, we saw overlaps in DEGs from the two cell types (glutamatergic neurons and astrocytes) with the most numbers of cells. It is also possible that the differences and similarities from the two gene sets are biologically significant, comparing the latent vulnerability state in animals that have not experienced chronic stress to those who have. No doubt there are many compensatory changes that happen in response to stress that manifest as a depressive state. It is possible that the overlapping genes between our two datasets point to genes that are pre-existing causal genes in the development of a depressive phenotype (Supplemental Table S7, column K). Interestingly, we observed little to no overlap when comparing with mice that had a recent stress exposure. However, we did observe more overlapping genes at a time further from the stress exposure (28 days post chronic social defeat). From these overlapping genes, we observed enrichment for ribosomal processes, which is consistent with a previous study that observed dysfunction in ribosomal gene expression in mice exposed to chronic social defeat stress in other brain regions [84]. Overall, these finding largely suggest that genes involved in stress vulnerability could be distinct from those altered by stress in susceptible animals.

In summary, this is the first study that has attempted to identify cells, transcriptional architecture, and biological processes involved in latent stress vulnerability in the PFC, an important regulatory hub in the brain involved in the development of stress-susceptible phenotypes. To do this, we used a novel approach of leveraging electrical brain-wide network activity (i.e. elevated *EF*1 activity) from multi-site in vivo recordings combined with single cell RNA-Seq to start to unravel the complex interplay of different cell types in mediating this brain state. While our study suggests that all major cell types are involve in the process, it highlights the importance of GABAergic neurons in this process and also sheds light on how microglia and mitochondrial activity could be involved in the development and maintenance of this brain state.

Acknowledgements

This work was supported by a NARSAD Young Investigator Grant from the Brain & Behavior Research Foundation (Rainbo Hultman). Additionally, this project received funding by 1DP2MH126377-01 (Rainbo Hultman), the Roy J. Carver Charitable Trust (Rainbo Hultman), and NINDS T32NS007124 (Yassine Filali and Micah Johnson). We would like to thank Jens Hjerling-Leffler and Hayley French for shared technical expertise. We thank Julia Miller for early technical support, and Neil Gallagher, Ted Abel, and Thomas

Nickl-Jockschat for helpful conversations. We thank the Iowa Institute of Human Genetics Genomics Division for training and use of equipment.

Figure Legends

Figure 1. Sorting animals by vulnerability brain states A) Experimental overview: from left to right implantation of multi-site in vivo electrodes, electrical recordings during forced interaction test (FIT) to measure *Electome Factor* 1 stress vulnerability network, single cell RNA-Seq, bioinformatic data analysis. B) LFP features of *Electome Factor* 1 C) *Electome Factor* 1 activity over time on FIT average of high (blue) and low (pink) clustering animals in bold with SEM in light blue and pink, respectively. D) *Electome Factor* 1 score clusters: low (pink), medium (green), and high (blue).

Figure 2. Single cell RNA-Seq cell type distributions A) t-distributed stochastic neighbor embedding (t-sne) plot of cells isolated from prefrontal cortex (PFC) from electrode-implanted animals. B) violin plot of cell-type specific markers C) cell type distribution by sex D) percentage cell types by high and low *Electome Factor* 1 network activity scores.

Figure 3. Differential Gene Expression and Gene Ontology Analyses in neurons Differential gene expression analysis conducted using ZINB-WaVE with sex as a covariate: A) volcano plot of differential gene expression between high and low *Electome Factor* 1 (stress vulnerability) scores in glutamatergic neurons B) gene ontology (GO) analysis for genes upregulated with high/low *Electome Factor* 1 scores in glutamatergic neurons C) gene ontology (GO) analysis for genes downregulated with high/low *Electome Factor* 1 scores in glutamatergic neurons D) volcano plot of differential gene expression between high and low Electome Factor 1 (stress vulnerability) scores in GABAergic neurons E) gene ontology (GO) analysis for genes upregulated with high/low *Electome Factor* 1 scores in GABAergic neurons F) gene ontology (GO) analysis for genes downregulated with high/low *Electome Factor* 1 scores in GABAergic neurons.

Figure 4. Differential Gene Expression and Gene Ontology Analyses in glial cells Differential gene expression analysis conducted using Zinbwave with sex as a covariate: A) volcano plot of differential gene expression between high and low *Electome Factor* 1 (stress vulnerability) scores in astrocytes B) astrocyte GO paths upregulated with higher EF1 scores C) astrocyte GO paths upregulated with lower EF1 scores D) volcano plot of differential gene expression between high and low *Electome Factor* 1 (stress vulnerability) scores in microglia E) microglia GO paths upregulated with higher EF1 scores F) microglia GO paths upregulated with lower EF1 scores G) volcano plot of differential gene expression between high and low *Electome Factor* 1 (stress vulnerability) scores in mature oligodendrocytes H) mature oligodendrocyte GO paths upregulated with higher EF1 scores I) mature oligodendrocyte GO paths upregulated with lower EF1 scores

Figure 5. Validation of ZINB-Wave Findings using DESingle For each cell type, from left to right is shown Venn Diagrams of overlapping genes between ZINB-Wave and DESingle, upregulated with EF1 (left), downregulated with EF1 (right), GSEA pathway analysis for enriched in genes with high EF1 (left), enrichment in genes for low EF1 (right). Data are show for A) glutamatergic neurons B) astrocytes C) GABAergic neurons D) microglia and E) mature oligodendrocytes.

Tables

Table 1. Differentially expressed genes identified by ZINB-Wave

Number of genes with padj < .05		
Cell Type	**up with high *EF1***	**up with low *EF1***
Astrocytes	341	221
GABAergic Neurons	242	140
Glutamatergic Neurons	838	548
Mature Oligodendrocytes	23	37
Microglia	46	77

References

1. McEwen, B.S. and H. Akil, *Revisiting the Stress Concept: Implications for Affective Disorders.* J Neurosci, 2020. **40**(1): p. 12-21.
2. Skene, N.G., et al., *Genetic identification of brain cell types underlying schizophrenia.* Nat Genet, 2018. **50**(6): p. 825-833.
3. Gass, N., et al., *Differential resting-state patterns across networks are spatially associated with Comt and Trmt2a gene expression patterns in a mouse model of 22q11.2 deletion.* Neuroimage, 2021. **243**: p. 118520.
4. Brainstorm, C., et al., *Analysis of shared heritability in common disorders of the brain.* Science, 2018. **360**(6395).
5. Cha, J. and I. Lee, *Single-cell network biology for resolving cellular heterogeneity in human diseases.* Exp Mol Med, 2020. **52**(11): p. 1798-1808.
6. Smeland, O.B., et al., *The emerging pattern of shared polygenic architecture of psychiatric disorders, conceptual and methodological challenges.* Psychiatr Genet, 2019. **29**(5): p. 152-159.
7. Sullivan, P.F., M.C. Neale, and K.S. Kendler, *Genetic epidemiology of major depression: review and meta-analysis.* Am J Psychiatry, 2000. **157**(10): p. 1552-62.
8. Krishnan, V., et al., *Molecular adaptations underlying susceptibility and resistance to social defeat in brain reward regions.* Cell, 2007. **131**(2): p. 391-404.
9. Bagot, R.C., et al., *Circuit-wide Transcriptional Profiling Reveals Brain Region-Specific Gene Networks Regulating Depression Susceptibility.* Neuron, 2016.
10. Covington, H.E., 3rd, et al., *Antidepressant effect of optogenetic stimulation of the medial prefrontal cortex.* J Neurosci, 2010. **30**(48): p. 16082-90.
11. Vialou, V., et al., *Prefrontal cortical circuit for depression- and anxiety-related behaviors mediated by cholecystokinin: role of DeltaFosB.* J Neurosci, 2014. **34**(11): p. 3878-87.
12. Lorsch, Z.S., et al., *Stress resilience is promoted by a Zfp189-driven transcriptional network in prefrontal cortex.* Nat Neurosci, 2019. **22**(9): p. 1413-1423.
13. Kumar, S., et al., *Cortical Control of Affective Networks.* J Neurosci, 2013. **33**(3): p. 1116 –1129.
14. Lee, E., et al., *Left brain cortical activity modulates stress effects on social behavior.* Sci Rep, 2015. **5**: p. 13342.
15. Seo, J.S., et al., *Cellular and molecular basis for stress-induced depression.* Mol Psychiatry, 2017. **22**(10): p. 1440-1447.
16. Shrestha, P., A. Mousa, and N. Heintz, *Layer 2/3 pyramidal cells in the medial prefrontal cortex moderate stress induced depressive behaviors.* Elife, 2015. **4**.
17. Ghosal, S., B. Hare, and R.S. Duman, *Prefrontal Cortex GABAergic Deficits and Circuit Dysfunction in the Pathophysiology and Treatment of Chronic Stress and Depression.* Curr Opin Behav Sci, 2017. **14**: p. 1-8.
18. Kelley, K.W., et al., *Variation among intact tissue samples reveals the core transcriptional features of human CNS cell classes.* Nat Neurosci, 2018. **21**(9): p. 1171-1184.
19. Gururajan, A., *The impact of chronic stress on the PFC transcriptome: a bioinformatic meta-analysis of publicly available RNA-sequencing datasets.* Stress, 2022. **25**(1): p. 305-312.
20. Gritti, D., et al., *Neuroinflammation in Major Depressive Disorder: A Review of PET Imaging Studies Examining the 18-kDa Translocator Protein.* J Affect Disord, 2021. **292**: p. 642-651.
21. Hultman, R., et al., *Brain-wide Electrical Spatiotemporal Dynamics Encode Depression Vulnerability.* Cell, 2018. **173**(1): p. 166-180 e14.
22. Dzirasa, K., et al., *Chronic in vivo multi-circuit neurophysiological recordings in mice.* J Neurosci Methods, 2011. **195**(1): p. 36-46.

23. Hultman, R., Mague, S.D., Li, Q., Katz, B.M., Michel, N., Lin, L., Wang, J., David, L.K., Blount, Chandy, R., Carlson, D., Ulrich, K., Carin, L., Dunson, Kumar, S., Deisseroth, K. Moore, S.D., Dzirasa, K., *Prefrontal Cortex-Mediated Slow-Evolving Limbic Dynamics Drives Stress-Induced Emotional Pathology.* Neuron, 2016. **In Press**.
24. Kumar, S., et al., *Prefrontal cortex reactivity underlies trait vulnerability to chronic social defeat stress.* Nat Commun, 2014. **5**: p. 4537.
25. Osorio, D. and J.J. Cai, *Systematic determination of the mitochondrial proportion in human and mice tissues for single-cell RNA-sequencing data quality control.* Bioinformatics, 2021. **37**(7): p. 963-967.
26. Germain, P.L., et al., *Doublet identification in single-cell sequencing data using scDblFinder.* F1000Res, 2021. **10**: p. 979.
27. Yao, Z., et al., *A taxonomy of transcriptomic cell types across the isocortex and hippocampal formation.* Cell, 2021. **184**(12): p. 3222-3241 e26.
28. Choudhary, S. and R. Satija, *Comparison and evaluation of statistical error models for scRNA-seq.* Genome Biol, 2022. **23**(1): p. 27.
29. Van den Berge, K., et al., *Observation weights unlock bulk RNA-seq tools for zero inflation and single-cell applications.* Genome Biol, 2018. **19**(1): p. 24.
30. Lun, A.T., D.J. McCarthy, and J.C. Marioni, *A step-by-step workflow for low-level analysis of single-cell RNA-seq data with Bioconductor.* F1000Res, 2016. **5**: p. 2122.
31. Love, M.I., Anders, S., Huber, W. *Analyzing RNA-seq data with DESeq2*. 2023 [cited 2023; Available from: http://bioconductor.org/packages/devel/bioc/vignettes/DESeq2/inst/doc/DESeq2.html.
32. Love, M.I., W. Huber, and S. Anders, *Moderated estimation of fold change and dispersion for RNA-seq data with DESeq2.* Genome Biol, 2014. **15**(12): p. 550.
33. Risso, D., et al., *A general and flexible method for signal extraction from single-cell RNA-seq data.* Nat Commun, 2018. **9**(1): p. 284.
34. Miao, Z., et al., *DEsingle for detecting three types of differential expression in single-cell RNA-seq data.* Bioinformatics, 2018. **34**(18): p. 3223-3224.
35. Wang, T., et al., *Comparative analysis of differential gene expression analysis tools for single-cell RNA sequencing data.* BMC Bioinformatics, 2019. **20**(1): p. 40.
36. Abrantes, A., et al., *Gene expression changes following chronic antipsychotic exposure in single cells from mouse striatum.* Mol Psychiatry, 2022. **27**(6): p. 2803-2812.
37. Yu, G., et al., *clusterProfiler: an R package for comparing biological themes among gene clusters.* OMICS, 2012. **16**(5): p. 284-7.
38. Koopmans, F., et al., *SynGO: An Evidence-Based, Expert-Curated Knowledge Base for the Synapse.* Neuron, 2019. **103**(2): p. 217-234 e4.
39. Rath, S., et al., *MitoCarta3.0: an updated mitochondrial proteome now with sub-organelle localization and pathway annotations.* Nucleic Acids Res, 2021. **49**(D1): p. D1541-D1547.
40. Ero, C., et al., *A Cell Atlas for the Mouse Brain.* Front Neuroinform, 2018. **12**: p. 84.
41. Bhattacherjee, A., et al., *Cell type-specific transcriptional programs in mouse prefrontal cortex during adolescence and addiction.* Nat Commun, 2019. **10**(1): p. 4169.
42. Subramanian, A., et al., *Gene set enrichment analysis: a knowledge-based approach for interpreting genome-wide expression profiles.* Proc Natl Acad Sci U S A, 2005. **102**(43): p. 15545-50.
43. Arnsten, A.F., *Stress signalling pathways that impair prefrontal cortex structure and function.* Nat Rev Neurosci, 2009. **10**(6): p. 410-22.
44. Page, C.E., et al., *Npas4 deficiency interacts with adolescent stress to disrupt prefrontal GABAergic maturation and adult cognitive flexibility.* Genes Brain Behav, 2018. **17**(6): p. e12459.

45. Guadagno, A., et al., *Effects of Early Life Stress on the Developing Basolateral Amygdala-Prefrontal Cortex Circuit: The Emerging Role of Local Inhibition and Perineuronal Nets.* Front Hum Neurosci, 2021. **15**: p. 669120.
46. Stevenson, C.W., et al., *Early life programming of hemispheric lateralization and synchronization in the adult medial prefrontal cortex.* Neuroscience, 2008. **155**(3): p. 852-63.
47. Czeh, B., et al., *Long-Term Stress Disrupts the Structural and Functional Integrity of GABAergic Neuronal Networks in the Medial Prefrontal Cortex of Rats.* Front Cell Neurosci, 2018. **12**: p. 148.
48. Ghosal, S., et al., *Ketamine rapidly reverses stress-induced impairments in GABAergic transmission in the prefrontal cortex in male rodents.* Neurobiol Dis, 2020. **134**: p. 104669.
49. Banasr, M., et al., *Characterization of GABAergic marker expression in the chronic unpredictable stress model of depression.* Chronic Stress (Thousand Oaks), 2017. **1**.
50. Zou, H.W., et al., *The GABA(B1) receptor within the infralimbic cortex is implicated in stress resilience and vulnerability in mice.* Behav Brain Res, 2021. **406**: p. 113240.
51. Funayama, Y., et al., *Antidepressant Response and Stress Resilience Are Promoted by CART Peptides in GABAergic Neurons of the Anterior Cingulate Cortex.* Biol Psychiatry Glob Open Sci, 2023. **3**(1): p. 87-98.
52. Chen, P., et al., *Prefrontal Cortex Corticotropin-Releasing Factor Neurons Control Behavioral Style Selection under Challenging Situations.* Neuron, 2020. **106**(2): p. 301-315 e7.
53. Radley, J.J., K.L. Gosselink, and P.E. Sawchenko, *A discrete GABAergic relay mediates medial prefrontal cortical inhibition of the neuroendocrine stress response.* J Neurosci, 2009. **29**(22): p. 7330-40.
54. Hou, X., et al., *GABAergic System in Stress: Implications of GABAergic Neuron Subpopulations and the Gut-Vagus-Brain Pathway.* Neural Plast, 2020. **2020**: p. 8858415.
55. Hodes, G.E., et al., *Individual differences in the peripheral immune system promote resilience versus susceptibility to social stress.* Proc Natl Acad Sci U S A, 2014. **111**(45): p. 16136-41.
56. Wood, S.K., et al., *Individual differences in reactivity to social stress predict susceptibility and resilience to a depressive phenotype: role of corticotropin-releasing factor.* Endocrinology, 2010. **151**(4): p. 1795-805.
57. Willmore, L., et al., *Behavioural and dopaminergic signatures of resilience.* Nature, 2022. **611**(7934): p. 124-132.
58. Muir, J., et al., *In Vivo Fiber Photometry Reveals Signature of Future Stress Susceptibility in Nucleus Accumbens.* Neuropsychopharmacology, 2018. **43**(2): p. 255-263.
59. Hayes, L.N., et al., *Prenatal immune stress blunts microglia reactivity, impairing neurocircuitry.* Nature, 2022. **610**(7931): p. 327-334.
60. Wu, Y., et al., *Microglia: Dynamic Mediators of Synapse Development and Plasticity.* Trends Immunol, 2015. **36**(10): p. 605-613.
61. Tay, T.L., et al., *Microglia Gone Rogue: Impacts on Psychiatric Disorders across the Lifespan.* Front Mol Neurosci, 2017. **10**: p. 421.
62. Frick, L.R., K. Williams, and C. Pittenger, *Microglial dysregulation in psychiatric disease.* Clin Dev Immunol, 2013. **2013**: p. 608654.
63. Sakai, M., et al., *Deficient Autophagy in Microglia Aggravates Repeated Social Defeat Stress-Induced Social Avoidance.* Neural Plast, 2022. **2022**: p. 7503553.
64. Dutcher, E.G., et al., *Early-life stress and inflammation: A systematic review of a key experimental approach in rodents.* Brain Neurosci Adv, 2020. **4**: p. 2398212820978049.
65. Calcia, M.A., et al., *Stress and neuroinflammation: a systematic review of the effects of stress on microglia and the implications for mental illness.* Psychopharmacology (Berl), 2016. **233**(9): p. 1637-50.

66. Block, C.L., et al., *Prenatal environmental stressors impair postnatal microglia function and adult behavior in males.* Cell Rep, 2022. **40**(5): p. 111161.
67. Bolton, J.L., et al., *Early stress-induced impaired microglial pruning of excitatory synapses on immature CRH-expressing neurons provokes aberrant adult stress responses.* Cell Rep, 2022. **38**(13): p. 110600.
68. Ali, A.T., et al., *Nuclear genetic regulation of the human mitochondrial transcriptome.* Elife, 2019. **8**.
69. Picard, M., et al., *An energetic view of stress: Focus on mitochondria.* Front Neuroendocrinol, 2018. **49**: p. 72-85.
70. Gimsa, U., et al., *Behavior and stress reactivity in mouse strains with mitochondrial DNA variations.* Ann N Y Acad Sci, 2009. **1153**: p. 131-8.
71. Petschner, P., et al., *Genes linking mitochondrial function, cognitive impairment and depression are associated with endophenotypes serving precision medicine.* Neuroscience, 2017.
72. Filiou, M.D. and C. Sandi, *Anxiety and Brain Mitochondria: A Bidirectional Crosstalk.* Trends Neurosci, 2019. **42**(9): p. 573-588.
73. Nasca, C., et al., *Childhood trauma and insulin resistance in patients suffering from depressive disorders.* Exp Neurol, 2019. **315**: p. 15-20.
74. Kasahara, T. and T. Kato, *What Can Mitochondrial DNA Analysis Tell Us About Mood Disorders?* Biol Psychiatry, 2018. **83**(9): p. 731-738.
75. Wang, Q. and Y. Dwivedi, *Transcriptional profiling of mitochondria associated genes in prefrontal cortex of subjects with major depressive disorder.* World J Biol Psychiatry, 2017. **18**(8): p. 592-603.
76. Nasca, C., et al., *L-acetylcarnitine causes rapid antidepressant effects through the epigenetic induction of mGlu2 receptors.* Proc Natl Acad Sci U S A, 2013. **110**(12): p. 4804-9.
77. Nasca, C., et al., *Acetyl-l-carnitine deficiency in patients with major depressive disorder.* Proc Natl Acad Sci U S A, 2018. **115**(34): p. 8627-8632.
78. Nasca, C., et al., *Role of the Astroglial Glutamate Exchanger xCT in Ventral Hippocampus in Resilience to Stress.* Neuron, 2017. **96**(2): p. 402-413 e5.
79. Nasca, C., et al., *Multidimensional predictors of antidepressant responses: Integrating mitochondrial, genetic, metabolic and environmental factors with clinical outcomes.* Neurobiol Stress, 2021. **15**: p. 100407.
80. Picard, M., et al., *Mitochondrial functions modulate neuroendocrine, metabolic, inflammatory, and transcriptional responses to acute psychological stress.* Proc Natl Acad Sci U S A, 2015. **112**(48): p. E6614-23.
81. Nasca, C., et al., *Multidimensional Predictors of Susceptibility and Resilience to Social Defeat Stress.* Biol Psychiatry, 2019. **86**(6): p. 483-491.
82. Brivio, P., et al., *Metabolomic signature and mitochondrial dynamics outline the difference between vulnerability and resilience to chronic stress.* Transl Psychiatry, 2022. **12**(1): p. 87.
83. Weger, M., et al., *Mitochondrial gene signature in the prefrontal cortex for differential susceptibility to chronic stress.* Sci Rep, 2020. **10**(1): p. 18308.
84. Smagin, D.A., et al., *Heterogeneity of Brain Ribosomal Genes Expression Following Positive Fighting Experience in Male Mice as Revealed by RNA-Seq.* Mol Neurobiol, 2018. **55**(1): p. 390-401.

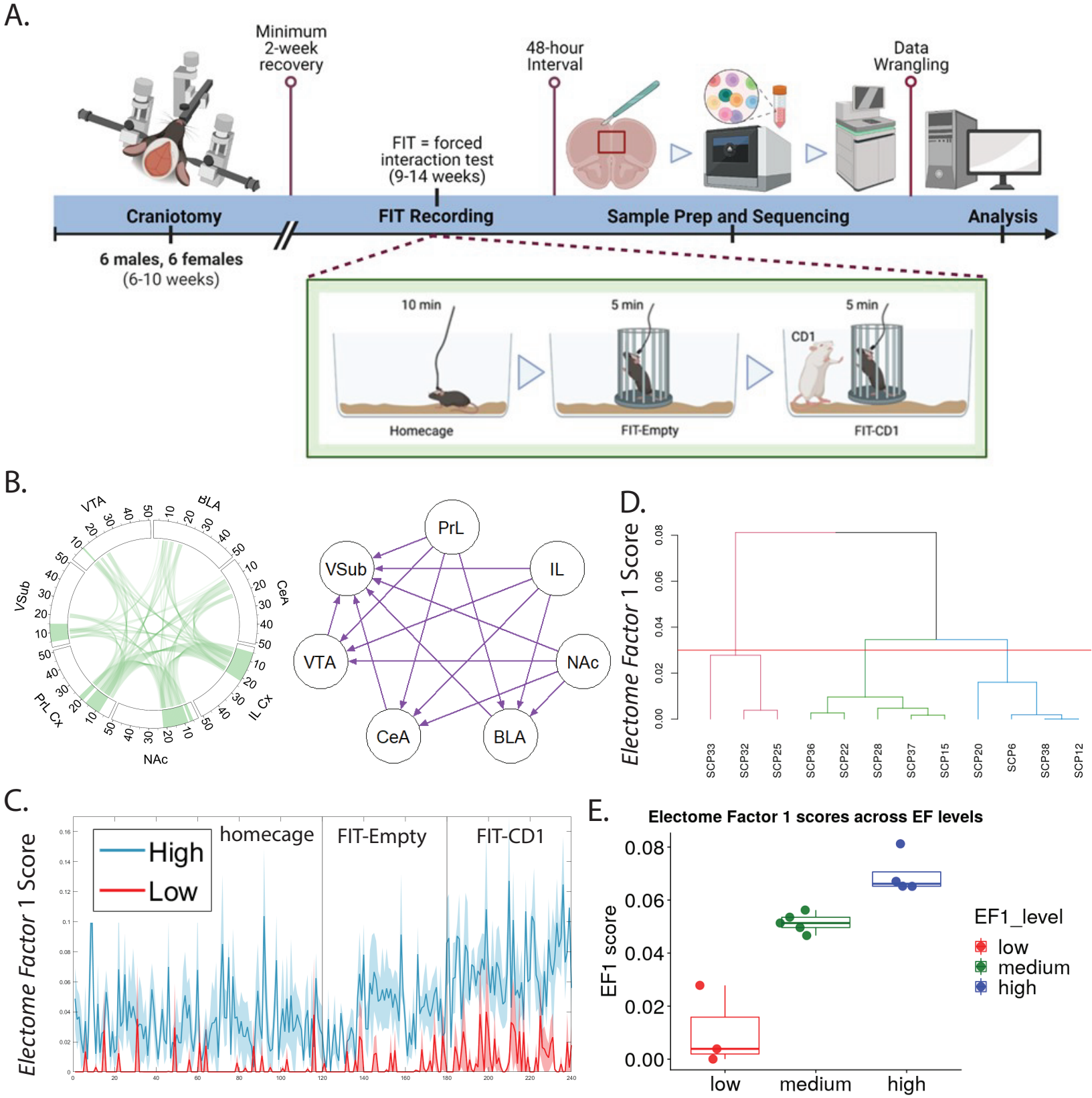
A.
Minimum 2-week recovery
48-hour Interval
Data Wrangling
FIT = forced interaction test (9-14 weeks)
Craniotomy
FIT Recording
Sample Prep and Sequencing
Analysis
6 males, 6 females (6-10 weeks)
10 min
5 min
5 min
CD1
Homecage
FIT-Empty
FIT-CD1
B.
VTA
BLA
CeA
IL Cx
NAc
PrL Cx
VSub
PrL
VSub
IL
VTA
NAc
CeA
BLA
D.
Electome Factor 1 Score
0.00
0.02
0.04
0.06
0.08
SCP33
SCP32
SCP25
SCP36
SCP22
SCP28
SCP37
SCP15
SCP20
SCP6
SCP38
SCP12
C.
Electome Factor 1 Score
High
Low
homecage
FIT-Empty
FIT-CD1
E.
Electome Factor 1 scores across EF levels
EF1 score
0.00
0.02
0.04
0.06
0.08
low
medium
high
EF1_level
low
medium
high

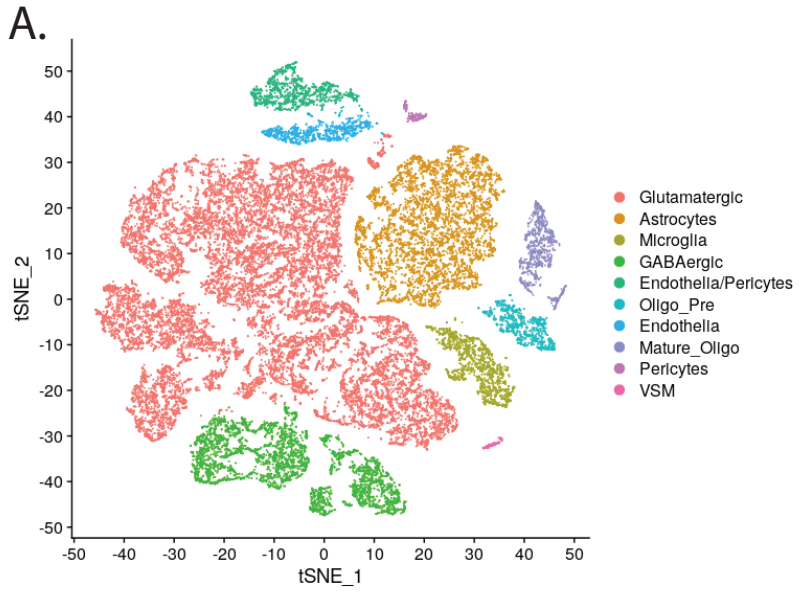
A.
tSNE_2
tSNE_1
Glutamatergic
Astrocytes
Microglia
GABAergic
Endothelia/Pericytes
Oligo_Pre
Endothelia
Mature_Oligo
Pericytes
VSM

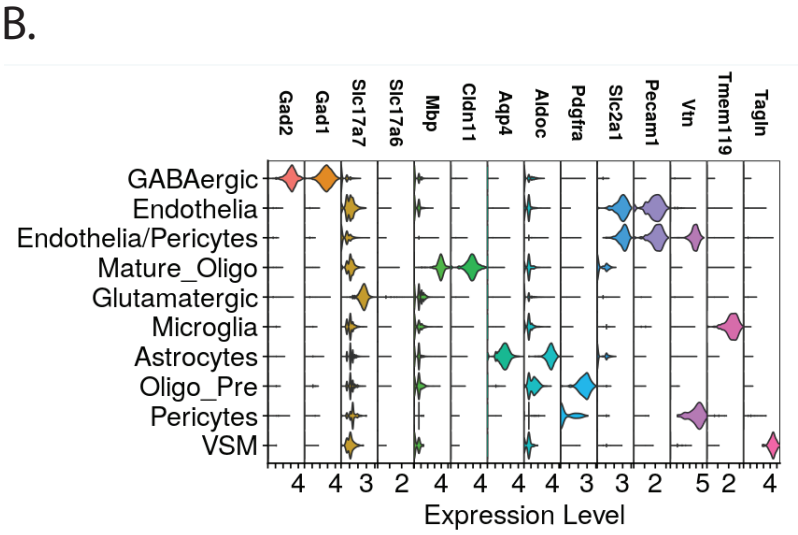
B.
Gad2
Gad1
Slc17a7
Slc17a6
Mbp
Cldn11
Aqp4
Aldoc
Pdgfra
Slc2a1
Pecam1
Vtn
Tmem119
Tagln
GABAergic
Endothelia
Endothelia/Pericytes
Mature_Oligo
Glutamatergic
Microglia
Astrocytes
Oligo_Pre
Pericytes
VSM
Expression Level

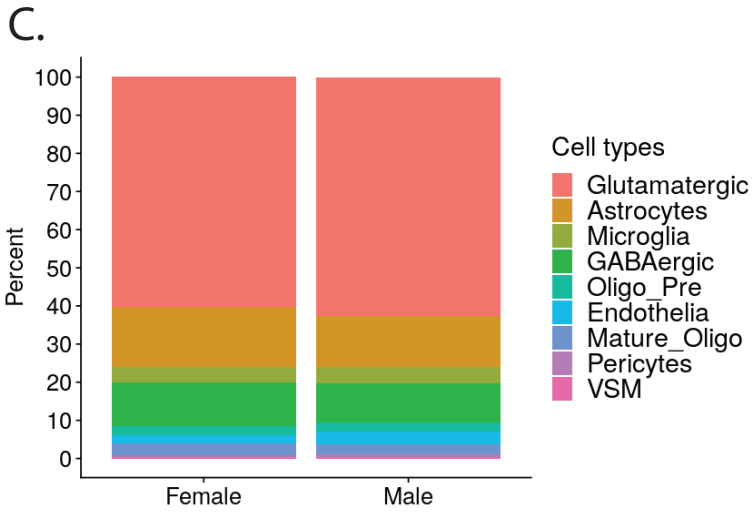
C.
Percent
Female
Male
Cell types
Glutamatergic
Astrocytes
Microglia
GABAergic
Oligo_Pre
Endothelia
Mature_Oligo
Pericytes
VSM

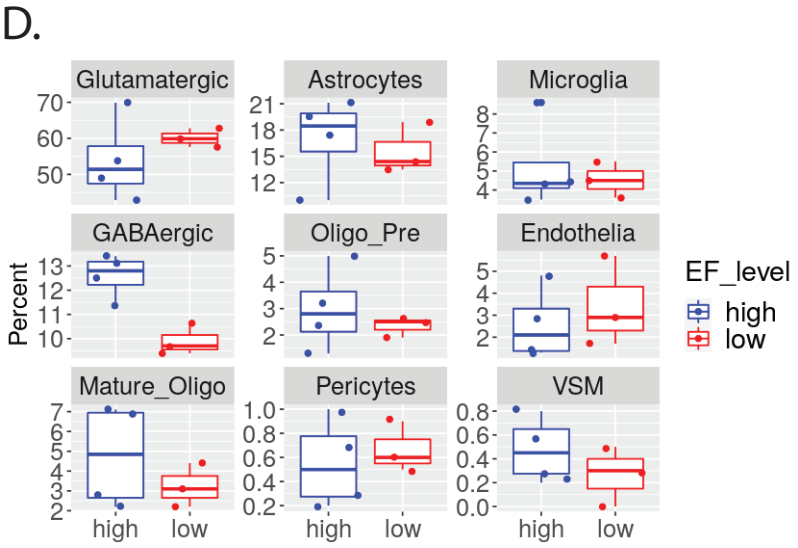
D.
Glutamatergic
Astrocytes
Microglia
GABAergic
Oligo_Pre
Endothelia
Mature_Oligo
Pericytes
VSM
Percent
high
low
EF_level
high
low

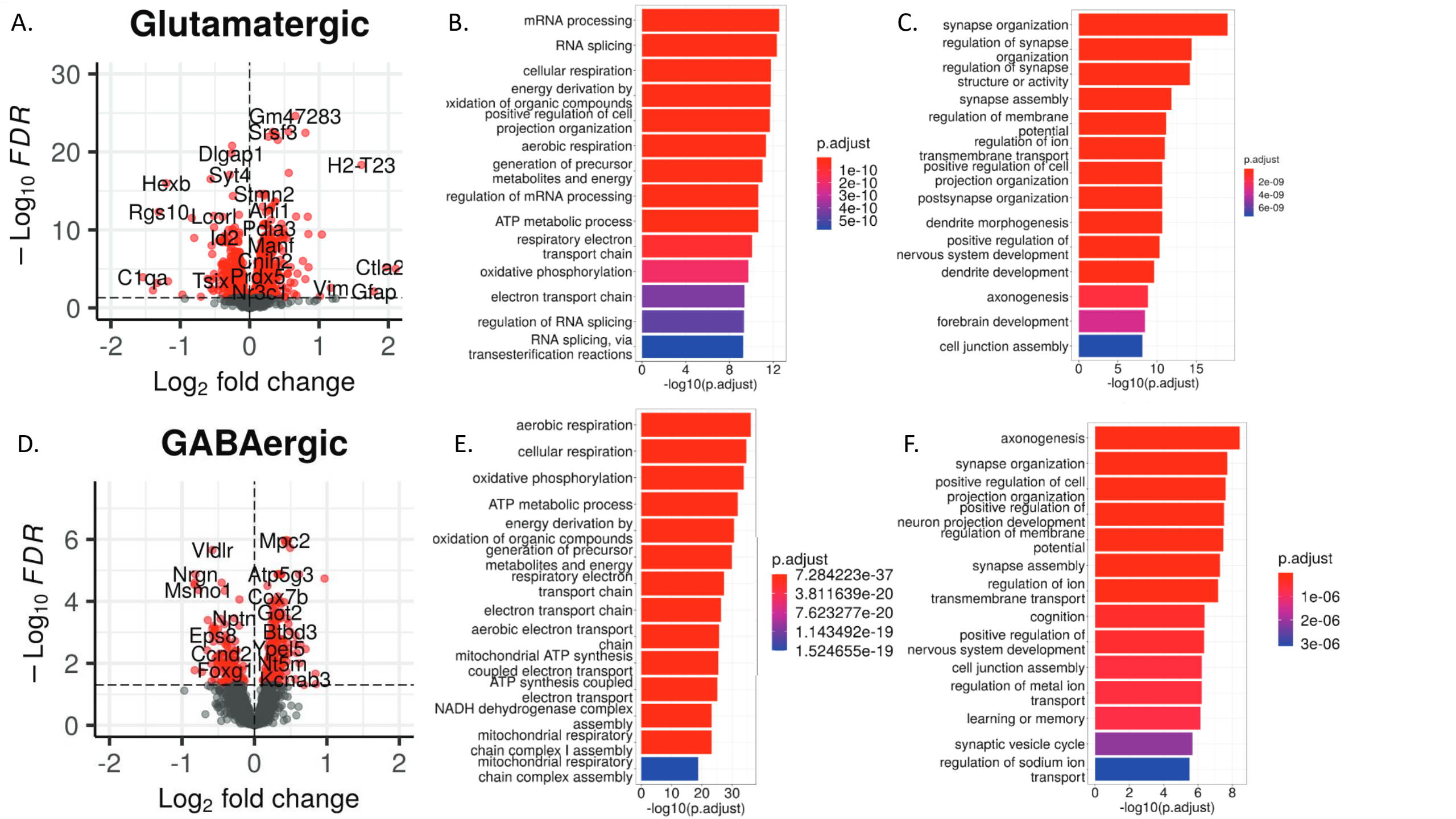
A.
Glutamatergic
−Log10 FDR
Log2 fold change
Gm47283
Srsf3
Dlgap1
H2-T23
Syt4
Hexb
Stmn2
Rgs10
Lcorl
Ahi1
Pdia3
Id2
Manf
Cnih2
Ctla2
C1qa
Tsix
Prdx5
Vim
Gfap
Nr3c1
B.
mRNA processing
RNA splicing
cellular respiration
energy derivation by oxidation of organic compounds
positive regulation of cell projection organization
aerobic respiration
generation of precursor metabolites and energy
regulation of mRNA processing
ATP metabolic process
respiratory electron transport chain
oxidative phosphorylation
electron transport chain
regulation of RNA splicing
RNA splicing, via transesterification reactions
-log10(p.adjust)
p.adjust
1e-10
2e-10
3e-10
4e-10
5e-10
C.
synapse organization
regulation of synapse organization
regulation of synapse structure or activity
synapse assembly
regulation of membrane potential
regulation of ion transmembrane transport
positive regulation of cell projection organization
postsynapse organization
dendrite morphogenesis
positive regulation of nervous system development
dendrite development
axonogenesis
forebrain development
cell junction assembly
-log10(p.adjust)
p.adjust
2e-09
4e-09
6e-09
D.
GABAergic
−Log10 FDR
Log2 fold change
Mpc2
Vldlr
Nrgn
Atp5g3
Msmo1
Cox7b
Got2
Nptn
Btbd3
Eps8
Ypel5
Ccnd2
Nt5m
Foxg1
Kcnab3
E.
aerobic respiration
cellular respiration
oxidative phosphorylation
ATP metabolic process
energy derivation by oxidation of organic compounds
generation of precursor metabolites and energy
respiratory electron transport chain
electron transport chain
aerobic electron transport chain
mitochondrial ATP synthesis coupled electron transport
ATP synthesis coupled electron transport
NADH dehydrogenase complex assembly
mitochondrial respiratory chain complex I assembly
mitochondrial respiratory chain complex assembly
-log10(p.adjust)
p.adjust
7.284223e-37
3.811639e-20
7.623277e-20
1.143492e-19
1.524655e-19
F.
axonogenesis
synapse organization
positive regulation of cell projection organization
positive regulation of neuron projection development
regulation of membrane potential
synapse assembly
regulation of ion transmembrane transport
cognition
positive regulation of nervous system development
cell junction assembly
regulation of metal ion transport
learning or memory
synaptic vesicle cycle
regulation of sodium ion transport
-log10(p.adjust)
p.adjust
1e-06
2e-06
3e-06

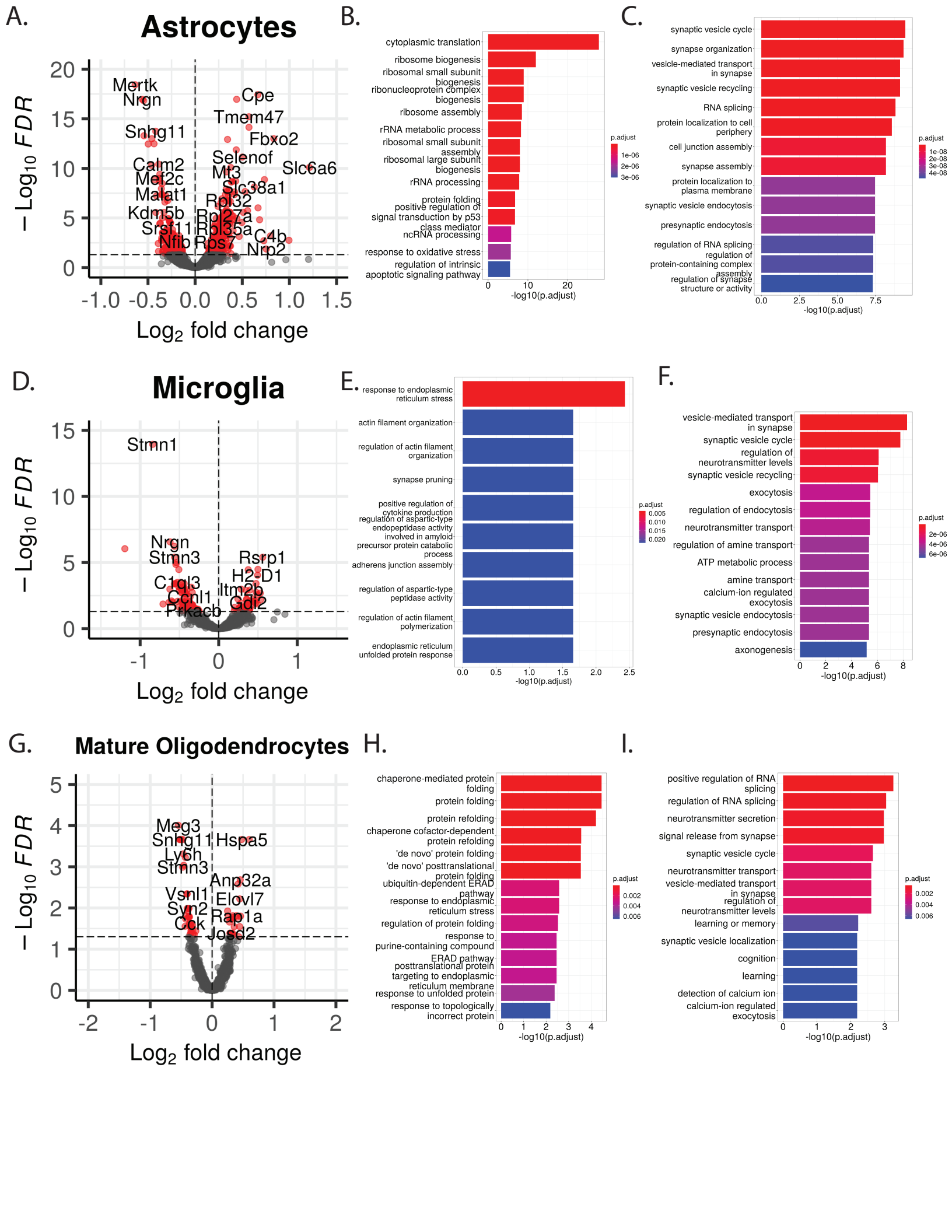
A.
Astrocytes
Mertk
Nrgn
Cpe
Tmem47
Snhg11
Fbxo2
Selenof
Calm2
Mt3
Slc6a6
Mef2c
Slc38a1
Malat1
Rpl32
Kdm5b
Rpl27a
Srsf11
Rpl35a
C4b
Nfib
Rps7
Nrp2
– Log10 FDR
Log2 fold change
B.
cytoplasmic translation
ribosome biogenesis
ribosomal small subunit biogenesis
ribonucleoprotein complex biogenesis
ribosome assembly
rRNA metabolic process
ribosomal small subunit assembly
ribosomal large subunit biogenesis
rRNA processing
protein folding
positive regulation of signal transduction by p53 class mediator
ncRNA processing
response to oxidative stress
regulation of intrinsic apoptotic signaling pathway
-log10(p.adjust)
p.adjust
1e-06
2e-06
3e-06
C.
synaptic vesicle cycle
synapse organization
vesicle-mediated transport in synapse
synaptic vesicle recycling
RNA splicing
protein localization to cell periphery
cell junction assembly
synapse assembly
protein localization to plasma membrane
synaptic vesicle endocytosis
presynaptic endocytosis
regulation of RNA splicing
regulation of protein-containing complex assembly
regulation of synapse structure or activity
-log10(p.adjust)
p.adjust
1e-08
2e-08
3e-08
4e-08
D.
Microglia
Stmn1
Nrgn
Stmn3
Rsrp1
H2-D1
C1ql3
Itm2b
Ccnl1
Gdi2
Prkacb
– Log10 FDR
Log2 fold change
E.
response to endoplasmic reticulum stress
actin filament organization
regulation of actin filament organization
synapse pruning
positive regulation of cytokine production
regulation of aspartic-type endopeptidase activity involved in amyloid precursor protein catabolic process
adherens junction assembly
regulation of aspartic-type peptidase activity
regulation of actin filament polymerization
endoplasmic reticulum unfolded protein response
-log10(p.adjust)
p.adjust
0.005
0.010
0.015
0.020
F.
vesicle-mediated transport in synapse
synaptic vesicle cycle
regulation of neurotransmitter levels
synaptic vesicle recycling
exocytosis
regulation of endocytosis
neurotransmitter transport
regulation of amine transport
ATP metabolic process
amine transport
calcium-ion regulated exocytosis
synaptic vesicle endocytosis
presynaptic endocytosis
axonogenesis
-log10(p.adjust)
p.adjust
2e-06
4e-06
6e-06
G.
Mature Oligodendrocytes
Meg3
Snhg11
Hspa5
Ly6h
Stmn3
Anp32a
Vsnl1
Elovl7
Syn2
Rap1a
Cck
Josd2
– Log10 FDR
Log2 fold change
H.
chaperone-mediated protein folding
protein folding
protein refolding
chaperone cofactor-dependent protein refolding
'de novo' protein folding
'de novo' posttranslational protein folding
ubiquitin-dependent ERAD pathway
response to endoplasmic reticulum stress
regulation of protein folding
response to purine-containing compound
ERAD pathway
posttranslational protein targeting to endoplasmic reticulum membrane
response to unfolded protein
response to topologically incorrect protein
-log10(p.adjust)
p.adjust
0.002
0.004
0.006
I.
positive regulation of RNA splicing
regulation of RNA splicing
neurotransmitter secretion
signal release from synapse
synaptic vesicle cycle
neurotransmitter transport
vesicle-mediated transport in synapse
regulation of neurotransmitter levels
learning or memory
synaptic vesicle localization
cognition
learning
detection of calcium ion
calcium-ion regulated exocytosis
-log10(p.adjust)
p.adjust
0.002
0.004
0.006

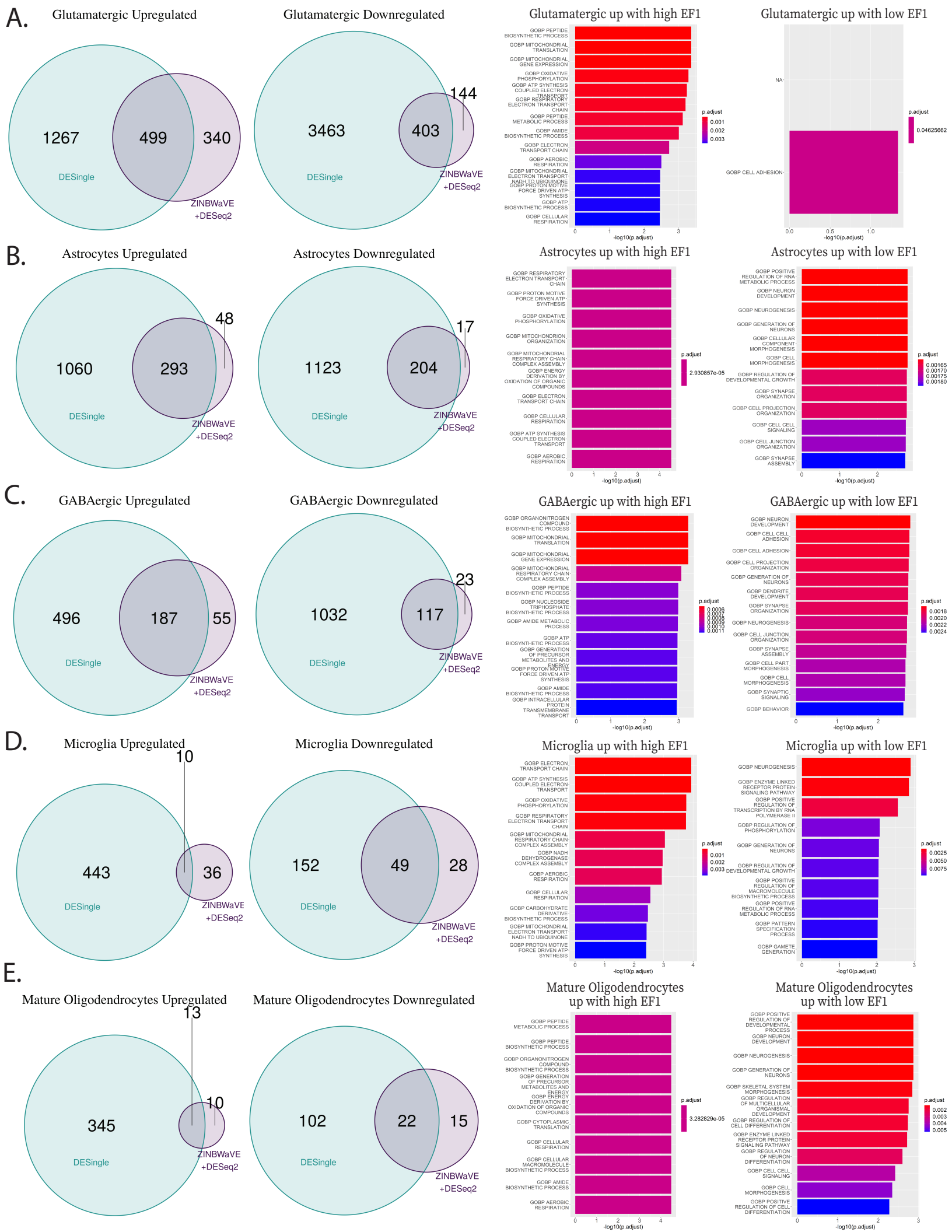
A.
Glutamatergic Upregulated
1267
499
340
DESingle
ZINBWaVE
+DESeq2
Glutamatergic Downregulated
3463
403
144
DESingle
ZINBWaVE
+DESeq2
Glutamatergic up with high EF1
GOBP PEPTIDE BIOSYNTHETIC PROCESS
GOBP MITOCHONDRIAL TRANSLATION
GOBP MITOCHONDRIAL GENE EXPRESSION
GOBP OXIDATIVE PHOSPHORYLATION
GOBP ATP SYNTHESIS COUPLED ELECTRON TRANSPORT
GOBP RESPIRATORY ELECTRON TRANSPORT CHAIN
GOBP PEPTIDE METABOLIC PROCESS
GOBP AMIDE BIOSYNTHETIC PROCESS
GOBP ELECTRON TRANSPORT CHAIN
GOBP AEROBIC RESPIRATION
GOBP MITOCHONDRIAL ELECTRON TRANSPORT NADH TO UBIQUINONE
GOBP PROTON MOTIVE FORCE DRIVEN ATP SYNTHESIS
GOBP ATP BIOSYNTHETIC PROCESS
GOBP CELLULAR RESPIRATION
p.adjust
0.001
0.002
0.003
-log10(p.adjust)
Glutamatergic up with low EF1
NA
GOBP CELL ADHESION
p.adjust
0.04625662
-log10(p.adjust)
B.
Astrocytes Upregulated
1060
293
48
DESingle
ZINBWaVE
+DESeq2
Astrocytes Downregulated
1123
204
17
DESingle
ZINBWaVE
+DESeq2
Astrocytes up with high EF1
GOBP RESPIRATORY ELECTRON TRANSPORT CHAIN
GOBP PROTON MOTIVE FORCE DRIVEN ATP SYNTHESIS
GOBP OXIDATIVE PHOSPHORYLATION
GOBP MITOCHONDRION ORGANIZATION
GOBP MITOCHONDRIAL RESPIRATORY CHAIN COMPLEX ASSEMBLY
GOBP ENERGY DERIVATION BY OXIDATION OF ORGANIC COMPOUNDS
GOBP ELECTRON TRANSPORT CHAIN
GOBP CELLULAR RESPIRATION
GOBP ATP SYNTHESIS COUPLED ELECTRON TRANSPORT
GOBP AEROBIC RESPIRATION
p.adjust
2.930857e-05
-log10(p.adjust)
Astrocytes up with low EF1
GOBP POSITIVE REGULATION OF RNA METABOLIC PROCESS
GOBP NEURON DEVELOPMENT
GOBP NEUROGENESIS
GOBP GENERATION OF NEURONS
GOBP CELLULAR COMPONENT MORPHOGENESIS
GOBP CELL MORPHOGENESIS
GOBP REGULATION OF DEVELOPMENTAL GROWTH
GOBP SYNAPSE ORGANIZATION
GOBP CELL PROJECTION ORGANIZATION
GOBP CELL CELL SIGNALING
GOBP CELL JUNCTION ORGANIZATION
GOBP SYNAPSE ASSEMBLY
p.adjust
0.00165
0.00170
0.00175
0.00180
-log10(p.adjust)
C.
GABAergic Upregulated
496
187
55
DESingle
ZINBWaVE
+DESeq2
GABAergic Downregulated
1032
117
23
DESingle
ZINBWaVE
+DESeq2
GABAergic up with high EF1
GOBP ORGANONITROGEN COMPOUND BIOSYNTHETIC PROCESS
GOBP MITOCHONDRIAL TRANSLATION
GOBP MITOCHONDRIAL GENE EXPRESSION
GOBP MITOCHONDRIAL RESPIRATORY CHAIN COMPLEX ASSEMBLY
GOBP PEPTIDE BIOSYNTHETIC PROCESS
GOBP NUCLEOSIDE TRIPHOSPHATE BIOSYNTHETIC PROCESS
GOBP AMIDE METABOLIC PROCESS
GOBP ATP BIOSYNTHETIC PROCESS
GOBP GENERATION OF PRECURSOR METABOLITES AND ENERGY
GOBP PROTON MOTIVE FORCE DRIVEN ATP SYNTHESIS
GOBP AMIDE BIOSYNTHETIC PROCESS
GOBP INTRACELLULAR PROTEIN TRANSMEMBRANE TRANSPORT
p.adjust
0.0006
0.0007
0.0008
0.0009
0.0010
0.0011
-log10(p.adjust)
GABAergic up with low EF1
GOBP NEURON DEVELOPMENT
GOBP CELL CELL ADHESION
GOBP CELL ADHESION
GOBP CELL PROJECTION ORGANIZATION
GOBP GENERATION OF NEURONS
GOBP DENDRITE DEVELOPMENT
GOBP SYNAPSE ORGANIZATION
GOBP NEUROGENESIS
GOBP CELL JUNCTION ORGANIZATION
GOBP SYNAPSE ASSEMBLY
GOBP CELL PART MORPHOGENESIS
GOBP CELL MORPHOGENESIS
GOBP SYNAPTIC SIGNALING
GOBP BEHAVIOR
p.adjust
0.0018
0.0020
0.0022
0.0024
-log10(p.adjust)
D.
Microglia Upregulated
443
36
10
DESingle
ZINBWaVE
+DESeq2
Microglia Downregulated
152
49
28
DESingle
ZINBWaVE
+DESeq2
Microglia up with high EF1
GOBP ELECTRON TRANSPORT CHAIN
GOBP ATP SYNTHESIS COUPLED ELECTRON TRANSPORT
GOBP OXIDATIVE PHOSPHORYLATION
GOBP RESPIRATORY ELECTRON TRANSPORT CHAIN
GOBP MITOCHONDRIAL RESPIRATORY CHAIN COMPLEX ASSEMBLY
GOBP NADH DEHYDROGENASE COMPLEX ASSEMBLY
GOBP AEROBIC RESPIRATION
GOBP CELLULAR RESPIRATION
GOBP CARBOHYDRATE DERIVATIVE BIOSYNTHETIC PROCESS
GOBP MITOCHONDRIAL ELECTRON TRANSPORT NADH TO UBIQUINONE
GOBP PROTON MOTIVE FORCE DRIVEN ATP SYNTHESIS
p.adjust
0.001
0.002
0.003
-log10(p.adjust)
Microglia up with low EF1
GOBP NEUROGENESIS
GOBP ENZYME LINKED RECEPTOR PROTEIN SIGNALING PATHWAY
GOBP POSITIVE REGULATION OF TRANSCRIPTION BY RNA POLYMERASE II
GOBP REGULATION OF PHOSPHORYLATION
GOBP GENERATION OF NEURONS
GOBP REGULATION OF DEVELOPMENTAL GROWTH
GOBP POSITIVE REGULATION OF MACROMOLECULE BIOSYNTHETIC PROCESS
GOBP POSITIVE REGULATION OF RNA METABOLIC PROCESS
GOBP PATTERN SPECIFICATION PROCESS
GOBP GAMETE GENERATION
p.adjust
0.0025
0.0050
0.0075
-log10(p.adjust)
E.
Mature Oligodendrocytes Upregulated
345
10
13
DESingle
ZINBWaVE
+DESeq2
Mature Oligodendrocytes Downregulated
102
22
15
DESingle
ZINBWaVE
+DESeq2
Mature Oligodendrocytes up with high EF1
GOBP PEPTIDE METABOLIC PROCESS
GOBP PEPTIDE BIOSYNTHETIC PROCESS
GOBP ORGANONITROGEN COMPOUND BIOSYNTHETIC PROCESS
GOBP GENERATION OF PRECURSOR METABOLITES AND ENERGY
GOBP ENERGY DERIVATION BY OXIDATION OF ORGANIC COMPOUNDS
GOBP CYTOPLASMIC TRANSLATION
GOBP CELLULAR RESPIRATION
GOBP CELLULAR MACROMOLECULE BIOSYNTHETIC PROCESS
GOBP AMIDE BIOSYNTHETIC PROCESS
GOBP AEROBIC RESPIRATION
p.adjust
3.282829e-05
-log10(p.adjust)
Mature Oligodendrocytes up with low EF1
GOBP POSITIVE REGULATION OF DEVELOPMENTAL PROCESS
GOBP NEURON DEVELOPMENT
GOBP NEUROGENESIS
GOBP GENERATION OF NEURONS
GOBP SKELETAL SYSTEM MORPHOGENESIS
GOBP REGULATION OF MULTICELLULAR ORGANISMAL DEVELOPMENT
GOBP REGULATION OF CELL DIFFERENTIATION
GOBP ENZYME LINKED RECEPTOR PROTEIN SIGNALING PATHWAY
GOBP REGULATION OF NEURON DIFFERENTIATION
GOBP CELL CELL SIGNALING
GOBP CELL MORPHOGENESIS
GOBP POSITIVE REGULATION OF CELL DIFFERENTIATION
p.adjust
0.002
0.003
0.004
0.005
-log10(p.adjust)